J. Micromech. Microeng. **23** (2013) 114008 (7pp) doi:10.1088/0960-1317/23/11/114008

Microfabricated nickel-based electrodes for high-power battery applications

A Armutlulu[1], **S A Bidstrup Allen**[1] **and M G Allen**[1,2]

[1] School of Chemical and Biomolecular Engineering, Georgia Institute of Technology, 311 Ferst Drive, Atlanta, GA 30332, USA
[2] School of Electrical and Computer Engineering, Georgia Institute of Technology, 791 Atlantic Drive, Atlanta, GA 30332, USA

E-mail: aarmutlulu3@gatech.edu

Received 4 April 2013, in final form 10 June 2013
Published 25 October 2013
Online at stacks.iop.org/JMM/23/114008

Abstract
High-surface area, three-dimensional (3D) microstructures are designed and fabricated by the sequential electroplating of sacrificial and structural layers in a photoresist mold. A conformal coating of electrochemically deposited nickel hydroxide ($Ni(OH)_2$) films on these MEMS-enabled multilayer structures enabled the formation of functional electrodes for electrochemical energy storage devices. The characterization of the electrodes is performed galvanostatically at various charge and discharge rates. Electrodes with a varying number of laminations are shown to yield areal capacities from 0.1 to 5.2 mAh cm^{-2}. Power characteristics of the electrodes are determined by applying ultra-high charge rates of up to 120 C. At this high charge rate, the electrode is able to deliver 90% of its capacity.

(Some figures may appear in colour only in the online journal)

1. Introduction

Over the past two decades, the widespread miniaturization of portable electronic equipment from smart phones to numerous multimedia tools has led to the need for similarly scaled energy storage devices, i.e. batteries that possess high energy densities. In addition, the rate of energy transport, i.e. power density, has become a crucial aspect for these devices, which require rapid charge and discharge capabilities. Conventional batteries have relatively high energy densities providing the systems with prolonged energy supply, yet usually lack similarly high power densities, which limit the rate of energy transfer. Capacitors, and more recently supercapacitors, on the other hand, possess extremely high power densities; however, the amount of energy they can store is rather limited compared to batteries. To narrow the application gap between these two energy storage mechanisms, batteries with rapid charge and discharge capabilities are required.

A significant improvement in the charge and discharge capabilities of Ni- and Li-based secondary batteries has been recently reported where the high-power performance relies on the high-surface-area three-dimensional (3D) bicontinuous electrodes hosting a conformal active layer coating sandwiched between rapid ion (i.e. electrolyte) and electron (i.e. current collector) transport routes [1]. 3D micro- and nanostructured materials with a similar concept and various architectures including pillar arrays, metal networks and nanofoams have also been fabricated via MEMS technologies [2–4]. When utilized as battery electrodes, they have exhibited superior performance to their 2D thin-film counterparts in terms of both energy and power densities [5, 6]. Yet they generally fall short of providing significant improvement simultaneously in both their energy and power capabilities.

In the study reported herein, the design and fabrication of a high-surface area, 3D electrode, composed of a well-ordered current collector with multiple layers of metal structures and conformal coating of electrochemically active material, has been demonstrated. Due to its relatively easier synthesis process and safer operating conditions compared to Li-ion systems, nickel oxyhydroxide (NiOOH) is selected as the active material. Two separate fabrication routes are proposed for the fabrication of low- and high-capacity applications. The fabricated electrodes are tested and characterized in alkaline electrolytes under galvanostatic conditions.

2. NiOOH/Ni(OH)$_2$ chemistry

Although Li-ion is the most popular battery chemistry for portable electronic systems, the NiOOH/Ni(OH)$_2$ chemistry is not only more easily integrated with MEMS processes (e.g., aqueous electrodeposition), but it is also a component of the popular NiMH battery chemistry. It exhibits a reversible charge storage redox chemistry comprising the diffusion of protons through the solid-state lattices of β-NiOOH and β-Ni(OH)$_2$ as shown in the following reactions:

$$\mathrm{Ni(OH)_2 + OH^- \rightarrow NiOOH + H_2O + e^-} \quad (1)$$

$$\mathrm{NiOOH + H_2O + e^- \rightarrow Ni(OH)_2 + OH^-} \quad (2)$$

where the former and latter reactions are associated with charging and discharging of the electrode, respectively [7]. Various methods exist in the literature to synthesize Ni(OH)$_2$. Nano-sized Ni(OH)$_2$ structures possessing various morphologies in the form of nanosheets, nanorods, nanoribbons, nanotubes and nanowires have been synthesized to obtain improved specific capacity [8–13]. Yet they are mainly in powder form, which makes their deposition on the current collector difficult. Binders with conductive additives need to be utilized in order to attach these particles to the current collectors. The inclusion of organic binder compounds results in poorer contact between the active material particles and the highly conductive metal backbone, or current collector, which negatively contributes to the internal resistance of the electrode and thus, leads to a reduced performance. Additionally, the existence of these organic materials adds to the mass and the volume of the electrode and hence, decreases its specific capacity. Moreover, when the current collector comprises meso- or even microporous material (e.g. Ni nanofoams) it is quite likely that the applied active material particles are unevenly disseminated in the highly porous structure, clogging the outer pores and generating dead spaces within the structure leading to inefficient utilization of the electrode during the charge and discharge processes. These particles may even damage the current collector, particularly if the structure lacks sufficient mechanical robustness as in the case of some microscale electrodes [3].

Considering all of these aspects, an attractive approach to combining the current collector with the active material is either through the electrodeposition of the active material onto the current collector or through the growth of active material directly on the current collector. The latter approach can be investigated by using either electrochemical growth or the spontaneous growth of the active material.

Electrochemical growth involves direct anodic oxidation of the Ni structures in alkaline solutions. This method, however, yields a relatively thin Ni(OH)$_2$ layer consisting of no more than two–three monolayers due to the self-limiting nature of hydroxide layer growth [14–16]. This amount of active material is not sufficient for energy storage applications. To overcome this issue, techniques involving high-frequency potential cycling conditions have been introduced where the macroscopic growth of relatively thick Ni(OH)$_2$ layers is achieved by applying periodic square-wave potentials at frequencies exceeding 1 kHz [17]. Yet the amount of active material obtained using this method is still much less than can be obtained via electrodeposition. A mechanism involving template-free growth of Ni(OH)$_2$ nanosheets on a Ni substrate in the absence of potentiometric conditions has been proposed [18]. This method enables the growth of significant amounts of active material for a given footprint area. However, in order to have exact control over the amount of active material to be synthesized, the reaction rates need to be well defined.

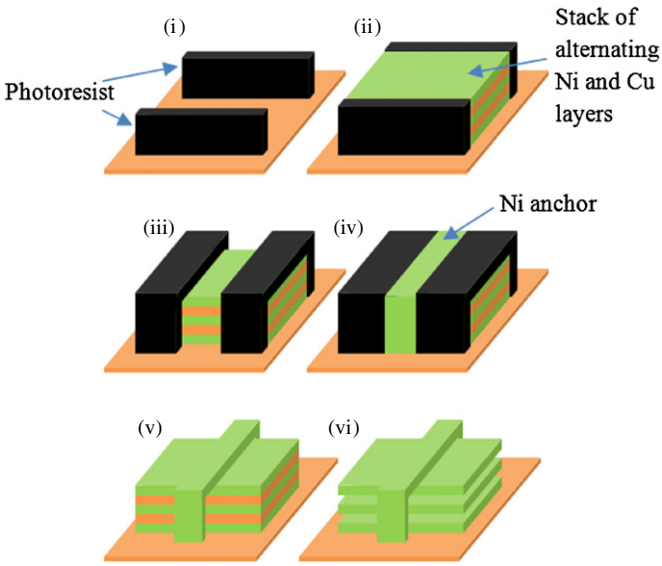

Figure 1. Fabrication schematic of the current collector demonstrating six major steps: (i) photoresist mold deposition and patterning, (ii) electroplating of alternating Ni and Cu layers, (iii) second photoresist mold patterning, (iv) electroplating of Ni anchor, (v) removal of photoresist, (vi) selective and complete etching of sacrificial Cu layers.

Electrodeposition can further be investigated under two main branches: anodic and cathodic deposition. There are numerous studies comprising both deposition techniques [19–34]. Our study is focused on cathodic deposition since a high-efficiency method has been developed for the active material deposition at room temperature, as well as a formula that accurately predicts the mass of the deposited active material [25, 34]. The active material has been reported to undergo a two-step reaction mechanism [25]. An equilibrium reaction takes place as shown in the following equation:

$$\mathrm{4Ni^{2+} + 4OH^- \leftrightarrow Ni_4(OH)_4^{4+}}. \quad (3)$$

This reaction is then followed by the deposition reaction of Ni(OH)$_2$ as given in the following equation:

$$\mathrm{Ni_4(OH)_4^{4+} + 4OH^- \rightarrow 4Ni(OH)_2 \downarrow}. \quad (4)$$

3. Development of the 3D electrodes

3.1. Fabrication of the current collector

Figure 1 illustrates the fabrication process of the current collector that involves the electroplating of alternating Ni and Cu layers followed by the removal of the sacrificial Cu layers resulting in a well ordered and highly laminated Ni structure. This process can be classified into two types: (i) fabrication

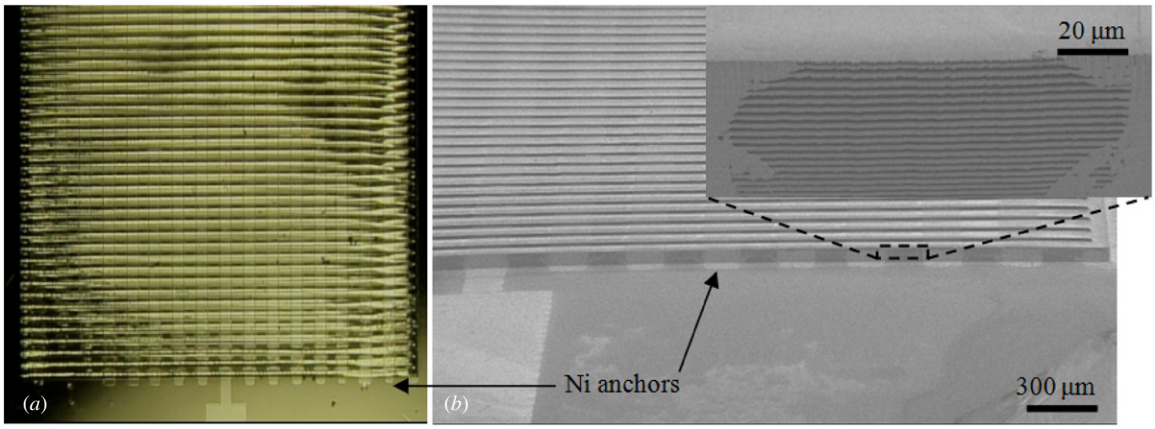

Figure 2. Optical and SEM images of the multilayer Ni backbone: (*a*) optical image illustrating the top view of the electrode where the vertical and horizontal lines represent the anchors and multilayer backbones, respectively, (ii) SEM image demonstrating the multilayer Ni backbone after complete removal of the selective Cu layers.

of current collectors with a total thickness of up to 100 μm for low-capacity applications and (ii) fabrication of current collectors with a total thickness of 300 μm and above for high-capacity applications. Both structures are fabricated on a 1 cm^2 footprint area. However, the differentiating factor is the choice of photoresist that serves as the mold in the electroplating process as detailed in the upcoming section. For high-capacity applications, highly laminated structures with up to 100 pairs of Ni/Cu layers are required in order to be able to deposit the required amount of active material on the structures. To achieve structures with that many layers, an ultra-thick, removable photoresist needs to be utilized as a mold. This ultra-thick photoresist can also be used for low-capacity applications. However, the long processing times required for various steps including soft-baking, UV lithography and stripping make it an unfavorable choice for low-capacity applications.

3.1.1. Fabrication of the low-capacity current collector. Ti/Cu/Ti layers are dc sputtered onto a glass substrate. Next, the substrate is spin-coated with a negative tone photoresist, NR21-20000P (Futurrex), that forms a film with an approximate thickness of 100 μm. This photoresist layer is then patterned via UV exposure (365 nm) and developed in an aqueous tetramethylammonium hydroxide (TMAH) solution (RD6, Futurrex) to serve as the mold during the electroplating process. Upon preparation of the mold, the topmost Ti layer is etched by diluted hydrofluoric acid so that the underlying Cu layer is exposed and utilized as a seed layer for the subsequent electroplating process. The electroplating of the alternating Ni and Cu layers is carried out in their respective electroplating baths where Ni and Cu serve as structural and sacrificial layers, respectively. For Ni deposition, an all-sulfate bath consisting of nickel sulfate ($NiSO_4$), boric acid (H_3BO_3) and saccharin is prepared, whereas a commercial electroplating solution is used for Cu deposition. The current density is set to 10 mA cm^{-2} for the deposition of both metals. A robotic plating setup, as described in our previous study, is used to perform repetitive alternating electroplating of tens of Ni/Cu pairs in a well-controlled fashion [5]. In order to avoid cross-contamination of the electroplating solutions, the substrate is rinsed in two separate deionized (DI) water baths between the electroplating of subsequent Ni and Cu layers. For highly laminated structures, the plating process might take up to 48 h. In such circumstances, the water in the rinsing baths is refreshed every 8 h.

Once the electroplating is completed, the photoresist mold is stripped with acetone. After rinsing thoroughly with DI water, the sample is immersed in a selective Cu etching solution for 1–2 min which enables a slight etching of Cu layers to a depth of 1–2 μm. This permits the anchor, which is electroplated in the subsequent step, to provide better mechanical support for the structural Ni layers. Following this brief etching step, a second spinning and patterning process is carried out using the same photoresist as before. This time, the photoresist serves as the mold for the electrodeposition of thick Ni anchors on specific regions of the sidewalls of the multilayer structures. These anchors not only maintain a mechanical support for the Ni layers to prevent them from collapsing following the complete etching of the sacrificial Cu layers, but also provide electrical connection between individual Ni layers. Upon completion of the anchor plating, the photoresist mold is again stripped via acetone. The last step for the fabrication process of the current collector involves the complete and selective removal of the sacrificial Cu layers. The sample is placed in the selective Cu etchant for approximately 10 h to ensure the complete removal of the sacrificial layers. Next, the sample is rinsed carefully in DI water and then immersed in isopropyl alcohol immediately before full drying in the oven. Exposing the sample to liquids with descending capillary forces minimizes the risk of potential deformations in the multilayer structure, particularly for the cases involving thin Ni layers [35]. Drying the sample in the oven at 65 °C for 1 h concludes the fabrication process for the current collector. Figure 2 shows optical and SEM images of a 25-layer current collector after complete removal of the sacrificial Cu layers. In certain cases, where the channels on the sidewalls of the Ni backbone are partially clogged, an additional electropolishing step is performed by applying anodic pulse currents to the substrate in a Ni plating bath for 30 min.

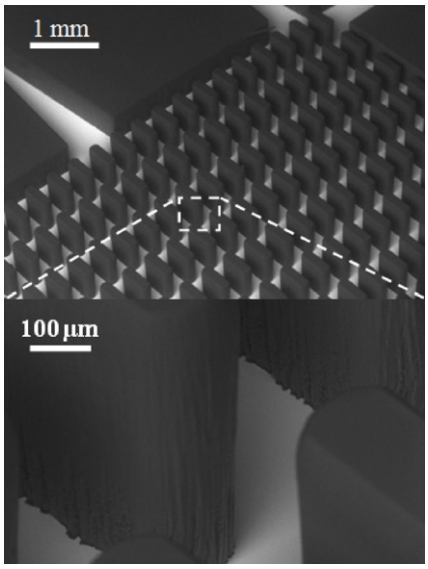

Figure 3. SEM images of the high aspect ratio mold before the electroplating process.

3.1.2. Fabrication of the high-capacity current collector. In order to improve the capacity of the electrode while keeping the electrode dimensions constant, a larger number of Cu/Ni electroplated layers are needed, which requires a thicker mold for the electroplating process. SU-8 has been known as a good candidate for the fabrication of such thick, high aspect ratio structures [36]. Once cross-linked, however, it becomes difficult to remove due to its rather high chemical resistance. Recently, an acrylic photoresist (AZ 125 nXT) has been shown to yield high aspect ratio (20:1) structures as thick as 1 mm and above [37]. The ability to remove this photoresist through wet stripping without the need for a plasma-assisted process has made it an attractive choice for our studies. With the exception of the mold preparation and stripping steps, the same processes as before are followed for the fabrication of the current collector. Hence, only the processing details of the photoresist are discussed here.

First, the photoresist with an approximate thickness of 1 mm is uniformly poured on the Ti/Cu/Ti coated glass substrate using a syringe. A very low spinning rate of 100 rpm is applied for 1 min to ensure further uniformity of the photoresist on the substrate. For these thick photoresist structures, a long pre-exposure bake is required. Care should be taken when performing soft baking because the amount of solvent in the resist should remain within a given range to ensure the necessary mechanical properties for further processing [37]. To estimate the amount of the remaining liquid, the weight of the sample is measured periodically. The optimum baking time at 105 °C has been found to be 14 h for this thickness of resist. After the soft baking process, the resist is cooled for 2 h at room temperature, which is followed by the UV exposure. For photoresist films with thicknesses exceeding hundreds of microns, prolonged exposure times are required which depend on the film thickness and feature size of the patterns. To ensure that necessary exposure has been applied, the energy dose is adjusted to 60 J cm^{-2}. Adhesion of the resist to the chrome mask during the long exposure process can be an issue since a significant amount of solvent still persists within the resist. To avoid this adhesion problem, a low-density polyethylene-based plastic film with a thickness of 12.5 μm is placed between the sample and the chrome mask. This thin plastic film has been estimated to cause the transmission of the UV light to diminish by approximately 10% which is taken into account when calculating the required time to apply the given amount of energy to the photoresist. Upon completion of the exposure, an ultrasonic-assisted development is carried out in a TMAH-based developer (AZ 300 MIF, AZ Electronic Materials) for about 30 min. The mold is then thoroughly rinsed and dried. Figure 3 shows the SEM images of the high aspect ratio photoresist mold. Immediately before the electroplating process, O_2 plasma treatment is performed to improve the wettability of the resist, which has been observed to affect the electroplating quality significantly, particularly for applications involving ultra-thick photoresist layers where the diffusion of the aqueous plating solution might be a limiting factor for the deposit quality.

Upon completion of the electroplating process, the photoresist is stripped. The bulk resist surrounding the multilayer structures can be easily removed via acetone. The pillars, however, need to be first treated with dimethyl sulfoxide solution at 80 °C for 30 min followed by ultrasonication in DI water for another 30 min. Optical images in figure 4 show the photoresist mold before and after the electrodeposition of the multilayer structure. The fabrication of the electrodes with 75 and 90 laminations was realized with this photoresist.

As opposed to high lateral aspect ratio structures used for the low-capacity applications where the photoresist mold has

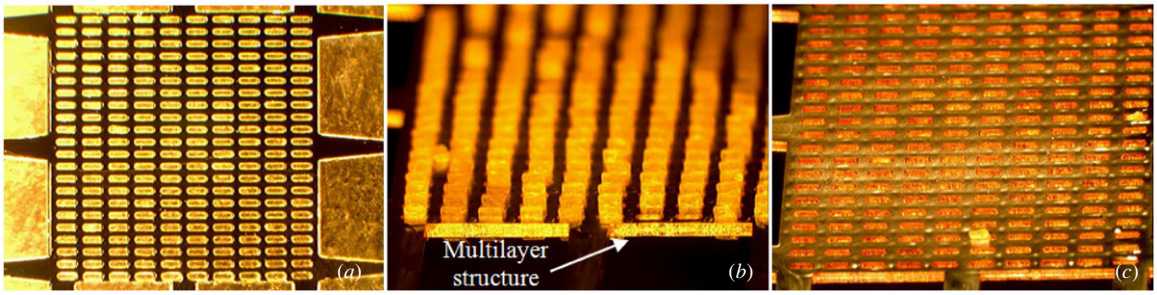

Figure 4. Optical images showing the ultra-thick mold: (*a*) top view of the array of high aspect ratio pillars before electroplating, (*b*) electroplated multilayer structure before the removal of the mold, (*c*) multilayer structure with etching holes exposed after the stripping of the mold.

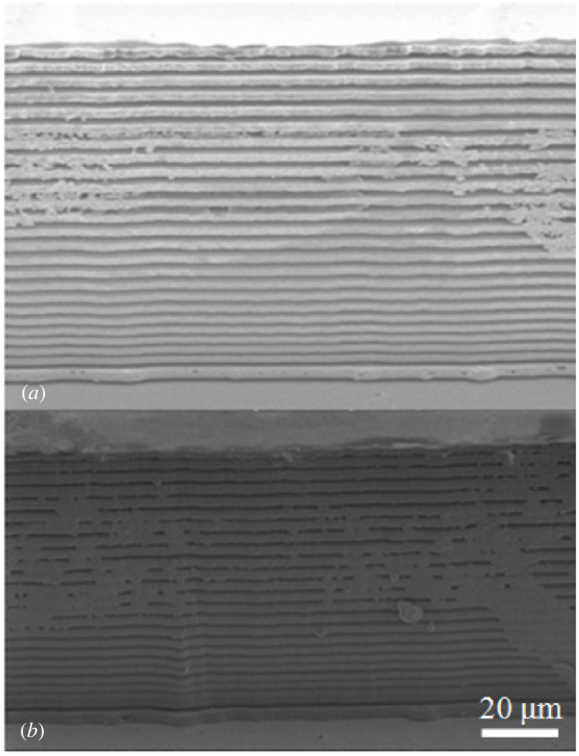

Figure 5. SEM images of the sidewall of the multilayer structure: (*a*) before and (*b*) after active material deposition.

a length and width of 10 mm and 0.1 mm, respectively, the mold should be patterned as laterally smaller size structures with pillar-shaped architectures as shown in figure 3 due to the stress-related limitations of AZ 125 nXT. The openings within the multilayer structures that arise after the removal of these pillars will serve as the etching holes during the selective Cu etching process.

3.2. Deposition of the active material

To demonstrate the improvement provided by these multilayer Ni structures to the battery performance, $Ni(OH)_2$ is deposited on these structures and used as the active material. The deposition of the active material onto the highly laminated Ni backbone is carried out galvanostatically in a 0.2 M nickel nitrate ($Ni(NO_3)_2$) solution. A two-electrode cell is prepared, using a Pt mesh as the counter electrode. Cathodic currents are applied to the substrate in pulses (1 s on/9 s off) in order to ensure the conformal coating of the Ni backbone. A microscale is used to weigh the sample before and after the electrodeposition process, and the amount of deposited active material is observed to be in good agreement with the theoretical value. SEM images of the 25-layer structure are shown in figure 5 where the sidewall of the multilayer backbone can be seen before and after $Ni(OH)_2$ deposition. It can be seen that the gaps between the layers are smaller in figure 5(*b*) than those in figure 5(*a*), confirming conformal deposition of the active material on the multilayer structure.

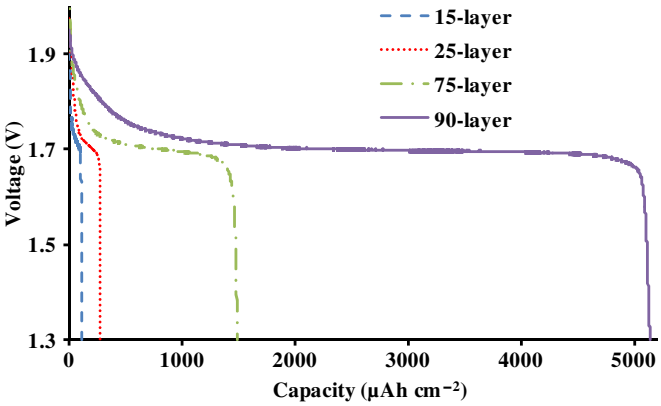

Figure 6. Performance of the electrodes with varying number of layers.

4. Charge and discharge characteristics of the NiOOH electrodes

To examine the charge and discharge characteristics of the fabricated electrodes, a two-electrode system is prepared in a 6M KOH electrolyte utilizing a large Zn sheet as the counter electrode, which forms a secondary Ni/Zn battery chemistry. Electrodes with varying number of laminations (15, 25, 75, and 90) are galvanostatically tested at room temperature. The electrodes are charged at various charging rates ranging from 2 to 120 C and then discharged at a constant rate of 2 C, where the x-C rate equals the rate at which the electrode is completely charged or discharged in $1/x$ hours. During these charge and discharge cycles, the potential between the multilayer Ni electrode and the Zn sheet is continuously recorded via a potentiostat (PowerLab 2/20, ADInstruments). The discharge process is terminated once the potential reduces to a cutoff value of 1.3 V. The limiting potential for charging is set to 2 V. From the discharge data, the capacity of the electrode is calculated by multiplying the discharge current by the time it takes for the potential to drop to the cutoff value. This value is then divided by the footprint area of 1 cm^2 for each electrode.

Discharge profiles of four electrodes with different number of laminations can be seen in figure 6. These profiles are in good agreement with the previously reported Ni/Zn batteries [38–40]. An interesting point to note is that the 15-layer structure exhibits an areal capacity of 0.1 mAh cm^{-2}, whereas a capacity of 5.2 mAh cm^{-2} is achieved with the 90-layer electrode. Therefore, a 6-fold increase in the number of layers resulted in more than 50-fold increase in the areal capacity. The underlying reason for the deviation from linearity is a result of the dimensions of the individual layers and active material films. In the latter case, the gap between two Ni layers, or in other words, the thickness of the sacrificial Cu layer before etching is approximately 4 μm, which allows more space to be occupied by the active material. However, having space for more active material is not always beneficial, particularly if the aim is enhanced power density. The thicker the active material on each Ni layer becomes, the longer is the path to diffuse for the solid-state ions which is likely to limit the charge and discharge rate of the electrode. Therefore, an optimum active material thickness needs to be determined

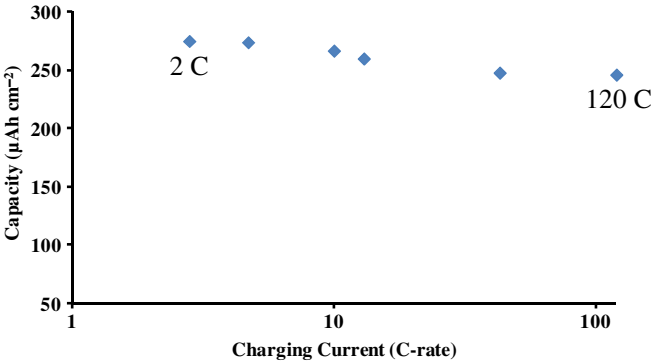

Figure 7. Areal capacity of the 25-layer electrode at various charge rates.

based on the energy and power needs of a given application where the capacity may have to be reduced at the offset of power or vice versa.

Figure 7 illustrates the relation between the areal capacity of a 25-layer electrode and the charging rate. The electrode is charged at six different rates ranging from 2 to 120 C and then discharged at a constant current of 2 mA in each cycle. As expected, a decay in the capacity is observed as the charge rate is increased. However, the capacity degradation of the electrode is greatly reduced when compared to its previously reported counterparts [27, 41]. The capacity obtained after the charge rate of 2 C is recorded as 0.28 mAh. When charged at 120 C, which corresponds to a charging time of 30 s, the areal capacity of the electrode is estimated to be 0.25 mAh referring to a 90% capacity retention even at such a high rate. The cycle life of the electrodes at high charge and discharge rates is also tested. The electrode is observed to deliver more than 82% of its initial capacity after cycling in excess of 80 times at a charge and discharge rate of 10 C.

5. Summary

The concept introduced in this study addresses several aspects of battery dynamics that are crucial for advanced battery performance. First, the high surface-to-volume ratio provides larger contact area between the electrode and the electrolyte, leading to higher number of active sites to host the redox reactions of the active material, which is vital particularly for high-power applications. Second, the conformal coating of a thin active material layer on the high-surface area structure reduces the path through which the diffusion of the solid-state ions of the active material (e.g., H^+) takes place. Therefore, the power-limiting effect of the low-conductivity active material (NiOOH) is significantly mitigated. Finally, the mechanically stable and electrochemically inert metallic backbone structure, serving also as a current collector with high electronic conductivity, exhibits minimum resistance for the transfer of electrons to and from the active material. The resulting electrodes yield areal capacities as high as 5.2 mAh cm^{-2}. More importantly, it is shown that the electrode is capable of delivering nearly 90% of its capacity even after ultra-fast charge rates of 120 C. This approach has the potential to be applied to commercially more attractive systems, such as Li-ion batteries, where a similar enhancement is expected in the charge and discharge performance of the system.

Acknowledgments

The authors would like to thank Dr Lawrence A Bottomley and Dr Leonardo Lizarraga for the provision of necessary equipment, as well as their technical support in electrochemical characterization of the electrodes.

References

[1] Zhang H G, Yu X D and Braun P V 2011 Three-dimensional bicontinuous ultrafast-charge and -discharge bulk battery electrodes *Nature Nanotechnol.* **6** 277–81
[2] Long J W, Dunn B, Rolison D R and White H S 2004 Three-dimensional battery architectures *Chem. Rev.* **104** 4463–92
[3] Arthur T S, Bates D J, Cirigliano N, Johnson D C, Malati P, Mosby J M, Perre E, Rawls M T, Prieto A L and Dunn B 2011 Three-dimensional electrodes and battery architectures *MRS Bull.* **36** 523–31
[4] Song M K, Park S, Alamgir F M, Cho J and Liu M L 2011 Nanostructured electrodes for lithium-ion and lithium-air batteries: the latest developments, challenges, and perspectives *Mater. Sci. Eng.* R **72** 203–52
[5] Armutlulu A, Fang Y, Kim S H, Ji C H, Allen S A B and Allen M G 2011 A MEMS-enabled 3D zinc-air microbattery with improved discharge characteristics based on a multilayer metallic substructure *J. Micromech. Microeng.* **21** 104011
[6] Nathan M, Golodnitsky D, Yufit V, Strauss E, Ripenbein T, Shechtman I, Menkin S and Peled E 2005 Three-dimensional thin-film Li-ion microbatteries for autonomous MEMS *J. Microelectromech. Syst.* **14** 879–85
[7] Han X J, Xu P, Xu C Q, Zhao L, Mo Z B and Liu T 2005 Study of the effects of nanometer beta-Ni(OH)(2) in nickel hydroxide electrodes *Electrochim. Acta* **50** 2763–9
[8] Matsui K, Kyotani T and Tomita A 2002 Hydrothermal synthesis of single-crystal Ni(OH)(2) nanorods in a carbon-coated anodic alumina film *Adv. Mater.* **14** 1216
[9] Liang Z H, Zhu Y J and Hu X L 2004 Beta-nickel hydroxide nanosheets and their thermal decomposition to nickel oxide nanosheets *J. Phys. Chem.* B **108** 3488–91
[10] Cai F S, Zhang G Y, Chen J, Gou X L, Liu H K and Dou S X 2004 Ni(OH)(2) tubes with mesoscale dimensions as positive-electrode materials of alkaline rechargeable batteries *Angew. Chem. Int. Edn Engl.* **43** 4212–6
[11] Coudun C and Hochepied J F 2005 Nickel hydroxide 'stacks of pancakes' obtained by the coupled effect of ammonia and template agent *J. Phys. Chem.* B **109** 6069–74
[12] Yang D N, Wang R M, He M S, Zhang J and Liu Z F 2005 Ribbon- and boardlike nanostructures of nickel hydroxide: synthesis, characterization, and electrochemical properties *J. Phys. Chem.* B **109** 7654–8
[13] Cao M H, He X Y, Chen J and Hu C W 2007 Self-assembled nickel hydroxide three-dimensional nanostructures: a nanomaterial for alkaline rechargeable batteries *Cryst. Growth Des.* **7** 170–4
[14] Wolf J F, Yeh L S R and Damjanovic A 1981 Anodic oxide-films at nickel electrodes in alkaline solutions—I. Kinetics of growth of the beta-$Ni(OH)_2$ phase *Electrochim. Acta* **26** 409–16

[15] Seghiouer A, Chevalet J, Barhoun A and Lantelme F 1998 Electrochemical oxidation of nickel in alkaline solutions: a voltammetric study and modelling *J. Electroanal. Chem.* **442** 113–23
[16] Alsabet M, Grden M and Jerkiewicz G 2011 Electrochemical growth of surface oxides on nickel. Part 1: formation of alpha-Ni(OH)(2) in relation to the polarization potential, polarization time, and temperature *Electrocatalysis* **2** 317–30
[17] Visintin A, Chialvo A C, Triaca W E and Arvia A J 1987 The electroformation of thick hydrous nickel hydroxide films through the application of periodic potential signals *J. Electroanal. Chem.* **225** 227–39
[18] Wang Y, Cao D X, Wang G L, Wang S S, Wen J Y and Yin J L 2011 Spherical clusters of beta-Ni(OH)(2) nanosheets supported on nickel foam for nickel metal hydride battery *Electrochim. Acta* **56** 8285–90
[19] Ord J L 1976 An optical study of the deposition and conversion of nickel hydroxide films *Surf. Sci.* **56** 413–24
[20] Tench D and Warren L F 1983 Electrodeposition of conducting transition metal oxide/hydroxide films from aqueous solution *J. Electrochem. Soc.* **130** 869–72
[21] Chen Y W D and Noufi R N 1984 Electrodeposition of nickel and cobalt oxides onto platinum and graphite electrodes for alkaline water electrolysis *J. Electrochem. Soc.* **131** 1447–51
[22] Carpenter M K, Conell R S and Corrigan D A 1987 The electrochromic properties of hydrous nickel oxide *Sol. Energy Mater.* **16** 333–46
[23] Morisaki S, Kawakami K and Baba N 1988 Formation of nickel oxyhydroxide thin films by electrodeposition and their electrochromic characteristics *Japan. J. Appl. Phys.* 1 **27** 314–8
[24] Corrigan D A and Knight S L 1989 Electrochemical and spectroscopic evidence on the participation of quadrivalent nickel in the nickel hydroxide redox reaction *J. Electrochem. Soc.* **136** 613–9
[25] Streinz C C, Hartman A P, Motupally S and Weidner J W 1995 The effect of current and nickel nitrate concentration on the deposition of nickel hydroxide films *J. Electrochem. Soc.* **142** 1084–9
[26] Motupally S, Streinz C C and Weidner J W 1998 Proton diffusion in nickel hydroxide—prediction of active material utilization *J. Electrochem. Soc.* **145** 29–34
[27] Lim H S and Verzwyvelt S A 1996 Effects of electrode thickness on power capability of a sintered-type nickel electrode *J. Power Sources* **62** 41–4
[28] Therese G H A and Kamath P V 2000 Electrochemical synthesis of metal oxides and hydroxides *Chem. Mater.* **12** 1195–204
[29] Kalu E E, Nwoga T T, Srinivasan V and Weidner J W 2001 Cyclic voltammetric studies of the effects of time and temperature on the capacitance of electrochemically deposited nickel hydroxide *J. Power Sources* **92** 163–7
[30] Tan Y W, Srinivasan S and Choi K S 2005 Electrochemical deposition of mesoporous nickel hydroxide films from dilute surfactant solutions *J. Am. Chem. Soc.* **127** 3596–604
[31] Nam K W, Lee E S, Kim J H, Lee Y H and Kim K B 2005 Synthesis and electrochemical investigations of $Ni_{1-x}O$ thin films and $Ni_{1-x}O$ on three-dimensional carbon substrates for electrochemical capacitors *J. Electrochem. Soc.* **152** A2123–9
[32] Wu M S, Huang Y A and Yang C H 2008 Capacitive behavior of porous nickel oxide/hydroxide electrodes with interconnected nanoflakes synthesized by anodic electrodeposition *J. Electrochem. Soc.* **155** A798–805
[33] Wu M S, Huang Y A, Jow J J, Yang W D, Hsieh C Y and Tsai H M 2008 Anodically potentiostatic deposition of flaky nickel oxide nanostructures and their electrochemical performances *Int. J. Hydrog. Energy* **33** 2921–6
[34] Streinz C C, Motupally S and Weidner J W 1995 The effect of temperature and ethanol on the deposition of nickel hydroxide films *J. Electrochem. Soc.* **142** 4051–6
[35] Matovic J 2006 Application of Ni electroplating techniques towards stress-free microelectromechanical system-based sensors and actuators *Proc. Inst. Mech. Eng.* C **220** 1645–54
[36] Kim J, Allen M G and Yoon Y K 2011 Computer-controlled dynamic mode multidirectional UV lithography for 3D microfabrication *J. Micromech. Microeng.* **21** 035003
[37] Staab M, Greiner F, Schlosser M and Schlaak H F 2011 Applications of novel high-aspect-ratio ultrathick UV photoresist for microelectroplating *J. Microelectromech. Syst.* **20** 794–6
[38] Humble P H, Harb J N and LaFollette R 2001 Microscopic nickel–zinc batteries for use in autonomous microsystems *J. Electrochem. Soc.* **148** A1357–61
[39] Iwakura C, Murakami H, Nohara S, Furukawa N and Inoue H 2005 Charge–discharge characteristics of nickel/zinc battery with polymer hydrogel electrolyte *J. Power Sources* **152** 291–4
[40] Gerasopoulos K, McCarthy M, Royston E, Culver J N and Ghodssi R 2008 Nanostructured nickel electrodes using the tobacco mosaic virus for microbattery applications *J. Micromech. Microeng.* **18** 104003
[41] Yao M, Okuno K, Iwaki T, Kato M, Harada K, Park J J, Tanase S and Sakai T 2007 Nickel substrate having three-dimensional micronetwork structure for high-power nickel/metal-hydride battery *Electrochem. Solid State Lett.* **10** A56–9